

DFT insights into the new Hf-based chalcogenide MAX phase Hf₂SeC

M. A. Ali^{a,*} Muhammad Waqas Qureshi^{b, c, **}

^aDepartment of Physics, Chittagong University of Engineering and Technology (CUET), Chattogram-4349, Bangladesh

^bState Key Laboratory of Advanced Welding and Joining, Harbin Institute of Technology, Harbin 150001, China

^cSchool of Materials Science & Engineering, Harbin Institute of Technology, Harbin 150001, China

Abstract

The physical characteristics of the novel chalcogenide MAX phase Hf₂SeC have been investigated using the DFT method. The obtained lattice constant and elastic constants (C_{ij}) are compared with previous results to check the consistency of our setting parameters during calculations. Moreover, the elastic properties such as elastic constants, moduli, anisotropy, and hardness are also compared with preexisting MAX phases of its kind. The checking of mechanical stability has been done based on C_{ij} in accordance with the previously stated stability criteria. The reason for the higher hardness of Hf₂SeC compared to Hf₂SC is explained using the density of states (DOS). The brittleness character of Hf₂SeC has been revealed using the Pugh ratio, Poisson's ratio, and Cauchy pressure. The electronic properties (band structure and charge density mapping) of Hf₂SeC are studied to disclose the metallic nature as well as bonding nature within the titled chalcogenide. The anisotropy in both electronic conductivity and mechanical properties is investigated. The temperature and pressure dependence of volume, Grüneisen parameter (γ), Debye temperature (Θ_D), thermal expansion coefficient (TEC), and specific heat at constant volume (C_V) are explored. In addition, minimum thermal conductivity (K_{min}) and melting point (T_m) are studied to explore its suitability for high-temperature applications.

Keywords: Hf₂SeC; Chalcogenide MAX phase; DFT study; Mechanical properties; Thermal properties;

1. Introduction

Recently, chalcogenide MAX phase members have been extended by the synthesis of two new chalcogens (Se) containing MAX phase: M₂SeC (M = Hf, Zr) [1,2]. The scientific community is trying to expand the family member of MAX phase materials for a long time, motivated by their peculiar properties, as a result, more than 150 MAX phases have already been revealed [3]. To do this, scientists have focused on the tuning of the compositions and structure to accomplish

superior properties. The recent attempts reported so far as new compounds [1,2,4–11] solid solutions [12–21]. Some other MAX phases have also been reported with slightly different structures: M_2A_2X [22–24] and M_3A_2X [25], rare-earth i-MAX phases [26,27], 212 MAX phases [28–31], 314 MAX phases [28,32,33]. The most recent extension of X element up to B has also been reported as MAX phase borides [5,6,34–39].

Now, the question is what aspect of the MAX phase triggers the scientists. The prime feature of the MAX phase that attracts mainly is the unification of metallic and ceramics properties. Again, the question is how it is possible to combine both characteristics. The answer lies within the structure of the MAX compounds in which there are M-A bonds responsible for metallic character and covalent M-X bonds that contribute to the ceramics character [40,41]; consequently, the conductivity (electrical and thermal), the strength of mechanical character, machinability are like metals, and the high-temperature mechanical parameters are good, corrosion and oxidation resistance also good as like as ceramics materials [42] which are exhibited by the MAX phases. Owing to the aforesaid characteristics, their potential applications include a very long list that can be found elsewhere [3,21,42–44].

The S containing MAX phases [M_2SC (M=Ti, Zr, Hf, Nb)] have been studied both experimentally and theoretically [5,6,35,45–50]. Bouhemadou et al [45] studied the elastic and electronic properties of M_2SC (M=Ti, Zr, Hf) phases. Superconducting phase Nb_2SC has been reported by Shein et al [46]. A comprehensive survey of elastic properties of the M_2AX phase was carried out by Cover et al [50] where S containing phases were included. Zr_2SC MAX compound was investigated by Feng et al in which the elastic and electronic properties were considered. Nasir et al [48,49] have selected Zr and Nb-based S containing phases for their DFT-based study. S-based MAX phase borides were synthesized by Rackl et al [5,6] which were further investigated [35]. To our knowledge, only the Zr_2SeC compound is studied experimentally [1] and theoretically [51]. Wang et al [2] synthesized Hf_2SeC and studied its thermal expansion coefficient and stiffness constants (C_{ij}) only. The obtained results were compared with those of Hf_2SC , Zr_2SeC , and Zr_2SC , Ti_2SC MAX phases where available. This too little information is not adequate to disclose the potential of Hf_2SeC for industrial use in various areas, in place of other MAX phases that are already been used. For example, the mechanical behavior exploring parameters such as elastic moduli, ductile/brittleness behavior,

mechanical hardness parameters are pre-requisite for the prediction of the applications as structural components at high-temperature [3,52,53]. Knowledge of Debye temperature, minimum thermal conductivity, Grüneisen parameter as well as melting temperature should be known to predict its high-temperature applications [54,55]. Calculation of electronic band structure, the density of states, and charge density mapping is very useful to disclose the bonding nature clearly and explain the mechanical and thermal properties. Thus, a comparative study of newly synthesized chalcogenide could be of scientific interest.

Therefore, we planned to perform a DFT-based investigation of the synthesized Hf₂SeC and the structural, elastic, electronic, and thermodynamic properties of Hf₂SeC are presented in this paper. To be more acceptable, the obtained results were compared with those of Hf₂SC, Zr₂SeC, Zr₂SC, and Nb₂SC MAX phases, where available.

2. Computational methodology

The results presented here are calculated using the Cambridge Serial Total Energy Package (CASTEP) code [56,57] based on the density functional theory. The generalized gradient approximation (GGA) of the Perdew–Burke–Ernzerhof (PBE) [58] type of functional was used as exchange and correlation term. The C - $2s^2 2p^2$, Se- $4s^2 4p^4$, and Hf - $5d^2 6s^2$ electronic orbitals were considered for pseudo-potential calculations. A k-point [59] mesh of size $12 \times 12 \times 4$ and the cutoff energy of 500 eV was used for the calculations. Further details of the calculations can be found elsewhere [51].

3. Results and discussion

3.1 Structural properties

The crystal structure of Hf₂SeC is presented in Fig. 1, it belongs to the hexagonal system and the space group is P6₃/mmc (194) [42]. The unit cell is composed of eight atoms, hence, its chemical formula revealed the two formula units. The octahedron Hf₆C is situated in between two atomic Se layers that can be shown in ref. [51]. The Wyckoff positions of M (Hf), A (Se), X (C) atoms are 4f ($1/3, 2/3, Z_M$), 2a ($1/3, 2/3, 3/4$) and 2c (0, 0, 0), respectively [60]. The physical properties of Hf₂SeC were further calculated after the geometrical relaxation of the unit cell. The cell parameters of the relaxed structure are given along with the previous experimental and theoretical results[2] to assure the setting of the parameters used for calculations. For example,

the obtained value of a is just 0.47% and c is just 0.88% larger than the experimental results. The discrepancy between the calculated values (present and previous) is much smaller (0.06% and 0.39% for a and c , respectively) compared to the experimental values.

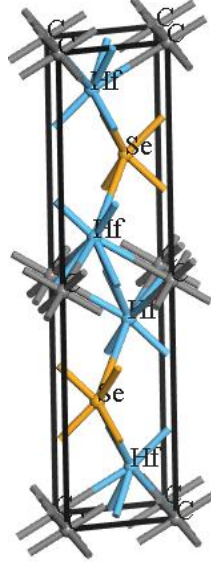


Fig. 1. Crystal structure (unit cell) of the Hf_2SeC compound.

Table 1. Calculated lattice parameters (a and c), c/a ratio, and atomic positions of Hf_2SeC MAX phase.

a (Å)	c (Å)	c/a	Ref.	Positions	Zr	Se	C
3.438	12.501	3.636	<i>This study</i>	x	1/3	1/3	0
3.422	12.391	3.621	<i>Expt.</i> [2]	y	2/3	2/3	0
3.436	12.452	3.624	<i>Theo.</i> [2]	z	0.0945	3/4	0
					0.0943 [2]		

3.3 Mechanical properties

Wang et al [2] calculated the stiffness constants only with an intention to correlate these with the thermal expansion coefficient of MAX phases. However, other important parameters like elastic moduli, failure mode based on Pugh/Poisson's ratio, mechanical hardness parameters, elastic anisotropic indices, etc. are remained unexplored and will be focused on in this section. To do this, we have re-calculated the stiffness constants (C_{ij}) of Hf_2SeC using the strain-stress method [30,32,61–63] and then used them further to investigate the other parameters mentioned above. The five independent stiffness constants of Hf_2SeC are given in Table 2 along with stiffness

constants of other S and Se-based MAX phases M_2AC ($M = \text{Hf, Zr, Nb}$, $A = \text{S, Se}$), where available. Though, Hf_2SeC is experimentally realized, the mechanical stability of Hf_2SeC is also checked by use of stiffness constants (C_{ij}) based on the Max Born [64] and Mouhat *et al.*[65] stability conditions as given here: $C_{11} > 0$, $C_{11} > C_{12}$, $C_{44} > 0$, $(C_{11} + C_{12})C_{33} - 2(C_{13})^2 > 0$. Since it (Hf_2SeC) is experimentally synthesized but for realistic use, checking of mechanical stability is mandatory. Table 2 confirms that the obtained C_{ij} s meet the stability conditions; hence, there is no doubt about the mechanical stability. In addition, C_{ij} s also provide knowledge regarding bonding strength along different axes, hardness, mechanical anisotropy, etc. For instance, the values C_{11} and C_{33} represent the stiffness along [100] and [001] directions. As evident from Table 2, C_{11} is smaller than C_{33} for all considered chalcogenide MAX phases implying lower deformation resistance along the a -axis than the c -axis. Moreover, C_{44} is lower than C_{33} and C_{11} , certifying an easy shear deformation compared to that of along the axial directions. Finally, the values of C_{11} , C_{33} , and C_{44} ($C_{11} \neq C_{33} \neq C_{44}$) confirmed the uneven bonding strength along with the a and c -axis as well as shear direction which is owing to the differences in the arrangement of atoms in different directions.

Table 2. The elastic constants, C_{ij} (GPa), bulk modulus, B (GPa), shear modulus, G (GPa), Young's modulus, Y (GPa), Hardness parameters, H_{Chen} (GPa) and H_{Miao} (GPa), Pugh ratio, G/B , Poisson ratio, ν and Cauchy Pressure, CP (GPa) of Hf_2SeC , along with those of Zr_2SeC and M_2SC ($M = \text{Zr, Hf, Nb}$).

Phase	C_{11}	C_{12}	C_{13}	C_{33}	C_{44}	B	G	Y	H_{Chen}	H_{Miao}	G/B	ν	CP	Reference
Hf_2SeC	287	77	98	306	130	158	113	273	18.47	21.69	0.72	0.21	-53	This study
	308	95	105	314	135									[2]
Hf_2SC	311	97	121	327	149	181	120	295	17.35	21.72	0.66	0.23	-52	[35]
Zr_2SeC	260	97	96	293	128	154	100	247	14.85	17.79	0.65	0.23	-30	[51]
Zr_2SC	295	89	102	315	138	166	115	280	17.89	21.57	0.69	0.22	-49	[35]
Nb_2SC	316	108	151	325	124	197	105	267	11.58	15.84	0.53	0.27	-16	[35]

The stiffness constants were then used to compute the Bulk modulus (B) and shear modulus (G) using Hill's approximation [66] which is the average of Voigt [67] and Reuss [68] models as follows:

$$B = (B_V + B_R)/2, \text{ where } B_V = [2(C_{11} + C_{12}) + C_{33} + 4C_{13}]/9 \text{ and}$$

$B_R = C^2/M$; $C^2 = C_{11} + C_{12})C_{33} - 2C_{13}^2$; $M = C_{11} + C_{12} + 2C_{33} - 4C_{13}$. B_V indicates the largest value of B (Voigt bulk modulus) and B_R express the lowest value of B (Reuss bulk modulus). Similarly, G was computed using the following equations:

$$G = (G_V + G_R)/2, \text{ where } G_V = [M + 12C_{44} + 12C_{66}]/30 \text{ and}$$

$$G_R = \left(\frac{5}{2}\right) [C^2 C_{44} C_{66}] / [3B_V C_{44} C_{66} + C^2 (C_{44} + C_{66})]; C_{66} = (C_{11} - C_{12})/2.$$

After then, the B and G were used to calculate the Young's modulus (Y) and Poisson's ratio (ν) using the following equations[35]: $Y = 9BG/(3B + G)$ and $\nu = (3B - Y)/(6B)$.

Finally, B , G , Y and ν were used to calculate the Hardness parameters using the equations [69,70]: $H_{\text{Chen}} = 2(k^2 G)^{0.585} - 3$ (where, Pugh's ratio, $k=G/B$) and $H_{\text{Miao}} = \frac{(1-2\nu)E}{6(1+\nu)}$.

Now, let us have a comparative discussion based on the values presented in Table 2. The value of C_{11} for Hf_2SeC is higher than that of another Se containing MAX phase, Zr_2SeC . On other hand, it is lower than those other S-based MAX phases, which is also true for C_{33} . Next, C_{44} of Hf_2SeC is higher than that of Zr_2SeC and Nb_2SC but lower than that M_2SC ($M = \text{Hf}, \text{Zr}$). As it is well known, C_{44} is a very good hardness predictor, i.e., more directly related to the elastic moduli compared to other stiffness constants and also used for the measurement of deformation resistance. Thus, according to the C_{44} , the compounds can be ranked as follows: $\text{Hf}_2\text{SC} > \text{Zr}_2\text{SC} > \text{Hf}_2\text{SeC} > \text{Zr}_2\text{SeC} > \text{Nb}_2\text{SC}$. Among the elastic moduli, G is a more accurate predictor for shear deformation compared to B and/or Y . The ranking of the compounds is same as for C_{44} , i.e., $\text{Hf}_2\text{SC} > \text{Zr}_2\text{SC} > \text{Hf}_2\text{SeC} > \text{Zr}_2\text{SeC} > \text{Nb}_2\text{SC}$. The Y is a good predictor for the stiffness measurement of the solids and the solid is said to be stiffer with a higher Y value. Thus, the compounds can be ranked as follows: $\text{Hf}_2\text{SC} > \text{Zr}_2\text{SC} > \text{Hf}_2\text{SeC} > \text{Nb}_2\text{SC} > \text{Zr}_2\text{SeC}$. However, the B of Nb_2SC somehow has the highest value. The ranking based on the B is also the same for other compounds except for Nb_2SC , i.e., $\text{Hf}_2\text{SC} > \text{Zr}_2\text{SC} > \text{Hf}_2\text{SeC} > \text{Zr}_2\text{SeC}$. Next, the hardness parameters using the Chen's [69] and Miao [70] formulae were calculated and presented in Table 2. As shown, The H_{Chen} of Hf_2SeC is comparatively higher than other chalcogenides presented here despite its lower values of elastic constants compared to Hf_2SC and Zr_2SC . The elastic constants don't reflect material's hardness directly, though, the parameters have usually higher values for harder solids. Thus, the titled chalcogenide is expected to be harder than the others presented here. H_{miao} of Hf_2SeC is also higher than that of other chalcogenides except for Hf_2SC where H_{miao} of Hf_2SeC is 0.13% lowered than that of Hf_2SC . In addition, Pan et al [71]

demonstrated that the Pugh ratio (which is also used in Chen's formula) is indirectly related to the Vickers hardness, which is highest for Hf_2SeC compared to other compounds considered here. It is noted that the hardness parameters of Hf_2SeC are lowered than that of Ti_2SC [32] ($H_{\text{Chen}}= 23.48$ GPa, $H_{\text{miao}}=29.85$ GPa, the elastic moduli are also higher) chalcogenide MAX phase. Thus, by taking into consideration the above facts, it is obvious to say that the titled compound possesses the 2nd highest hardness among the chalcogenide MAX phases. Despite the explanation stated above, still, the mystery (hardness of Hf_2SC is lower than that of Hf_2SeC though the stiffness constants and elastic moduli are higher) should be solved by further clarification in terms of the total density of states (DOS).

To check the ductility/brittleness character we used three well formalisms. Pugh ratio (G/B), the ratio of bulk to shear modulus, is a well-accepted parameter to separate the ductile and brittle materials with a critical value of 0.571. A value of G/B greater than 0.571 implies the brittleness character of solids and vice versa [72]. As evident, the titled MAX phase is brittle like its precursor Hf_2SC . The Poisson's ratio [73] is another parameter used to define a solid either ductile or brittle with a critical value of 0.26. Values lower than 0.26 indicate the brittleness character of solids and vice versa. It is seen in Table 2, that the titled phase is brittle again. Next, the Cauchy pressure [74] is also used to define a material either ductile or brittle. Values of a negative sign indicate the brittle solids while the positive sign indicates the ionic ductile solids. Table 2 revealed that the titled Se based MAX phase is brittle. A large negative value also indicates the dominant nature of a covalent bond in which a mixture of bonding is present. Thus, the covalent bond is dominant in the Hf_2SeC MAX phase where a mixture of covalent and ionic bonding is present.

3.3 Electronic properties

Fig. 2 (a) shows the DOS of Hf_2SeC and Hf_2SC in which black vertical lines indicate the peaks in the DOS of Hf_2SeC and red lines indicate the peaks in the DOS of Hf_2SC . The reference lines clearly indicate the peak shifting to the left when we go from S to Se. The peaks in the DOS are the results of hybridization among the different states involved in solids. The strength of the bonding between states depends on the position. The peak in the low energy sides, higher the bonding strength[19,35,75]. Thus, the bonding among the states in Hf_2SeC is expected to be

stronger compared to Hf_2SC as a consequence, the hardness of Hf_2SeC is also expected to be higher compared to Hf_2SC that is found in the present study. In addition, the DOS at the Fermi level is around 1.33 states/eV/cell for both phases, which implies the metallic nature of Hf_2SeC . To confirm electronic conductivity, we have calculated the electronic band structure presented in the following section.

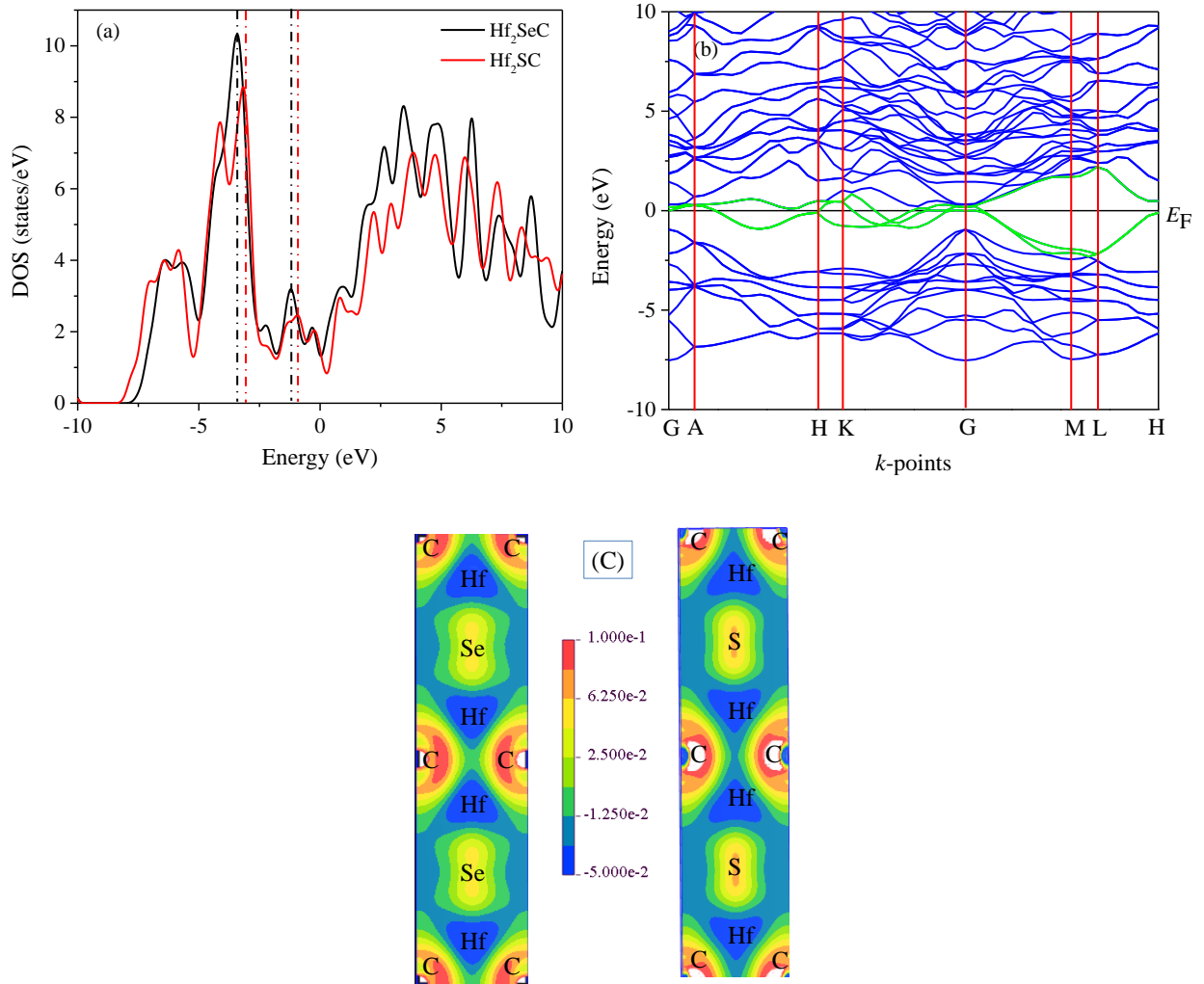


Fig. 1 (a) The DOS of Hf_2AC (A = Se, S), (b) electronic band structure of Hf_2SeC and (c) charge density mapping of Hf_2AC (A = Se, S).

The electronic band structure is also an important result concerning its electronic conductivity. The electronic band structure of Hf_2SeC calculated from the relaxed structure is shown in Fig. 2 (b) along the high symmetry lines: Γ -A-H-K- Γ -M-L-H. Like all other MAX phases[76], Hf_2SeC also exhibits metallic nature that can be confirmed from the band structure in which

overlapping of valence and conduction band is observed. Another interesting character is also noticed from the band structure, the energy dispersion along (*c*-direction): Γ -A, K-H, and L-M directions are smaller compared to the energy dispersion (basal plane): H-K, Γ -M, and L-H, thus, the electronic conductivity is not equal in the basal plane and *c*-direction. Smaller energy dispersion is owing to the higher electronic effective mass tensor that leads to a smaller conductivity and vice versa [19]. Thus, the typical conductivity nature for MAX phases [19,30,77] is also exhibited by Hf₂SeC: higher conductivity is observed in the basal plane in comparison with that of *c*-direction.

Fig. 2 (c) displays the CDM (in the units of e/Å³) in the (100) crystallographic plane which is designed to explore the nature of the bonding among the different atoms for Hf₂SeC and Hf₂SC. The positions of the atoms are denoted in the figure. As evident, the Hf-C bonding is a purely covalent bond like other MAX phases. The Hf-Se/S bonding is a mixture of a covalent and ionic type which is also another common nature for MAX phase materials. The replacement of A atom from Se to S results in a considerable change in the CDMs. As seen, the charge density (CD) at A (S) position increases. Thus, the common bonding nature of MAX phases is revealed by CDM for both Hf₂AC (A = Se, S) which is responsible for the combined properties of metals and ceramics.

3.4 Mechanical anisotropy

Because of the layered hexagonal symmetry for the MAX phase materials, the atomic arrangement is different along *a* and *c*-direction, consequently, unequal values of the C_{11} and C_{33} are obtained (Table 2). As a further consequence, mechanical anisotropy is observed like other MAX phases [30,32,78–80]. The important phenomena such as microcracks and anisotropic plastic deformation are the results of the mechanical anisotropy that shows a significant contribution in realizing the mechanical stability of the solids in extreme conditions. Due to the aforementioned reasons, the anisotropic nature of the mechanical properties characterizing parameters has been studied. To do this, We have calculated the different anisotropic factors for the {100}, {010} and {001} directions calculated using the equations[81]:

$$A_1 = \frac{1/6(C_{11}+C_{12}+2C_{33}-4C_{13})}{C_{44}}, A_2 = \frac{2C_{44}}{C_{11}-C_{12}}, A_3 = A_1 \cdot A_2 = \frac{1/3(C_{11}+C_{12}+2C_{33}-4C_{13})}{C_{11}-C_{12}}$$

The obtained values are presented in Table 3 along with other chalcogenide MAX phase carbides that confirm the anisotropy of Hf₂SeC where the non-zero values of A_i's indicating the level of anisotropy. The B along *a* and *c*-direction are estimated using the relations $B_a = a \frac{dP}{da} = \frac{\Lambda}{2+a}$ and $B_c = c \frac{dP}{dc} = \frac{B_a}{\alpha}$, respectively [82] where $\Lambda = 2(C_{11} + C_{12}) + 4C_{13}\alpha + C_{33}\alpha^2$ and $\alpha = \frac{(C_{11}+C_{12})-2C_{13}}{C_{33}-C_{13}}$. As evident from Table 3, $B_a \neq B_c$ means the B of Hf₂SeC is anisotropic in nature. The linear compressibility (*k*) along the *a* and *c*-axis is estimated by the equation [83]:

$$\frac{k_c}{k_a} = C_{11} + C_{12} - 2C_{13} / (C_{33} - C_{13})$$

The ratio of k_c/k_a is not one (1) (k_c/k_a is equal to 1 for isotropic materials) that confirms the anisotropic nature of Hf₂SeC. The universal anisotropic index A^U is estimated by the following equation [84]:

$$A^U = 5 \frac{G_V}{G_R} + \frac{B_V}{B_R} - 6 \geq 0 \quad (15)$$

where *B* and *G* are obtained by Voigt and Reuss models. Since, the values of A^U are greater than zero, indicating the anisotropic nature of Hf₂SeC. At end of this section, it is seen that the titled chalcogenide exhibits anisotropy in its elastic properties like other chalcogenide MAX phase carbides (Table 3).

Table 3. The anisotropic factors, A_1 , A_2 , A_3 , B_a , B_c , k_c/k_a , and universal anisotropic index A^U of M₂AC (M=Hf, Zr; A = Se, S) and Nb₂SC.

Phase	A_1	A_2	A_3	k_c/k_a	B_a	B_c	A^U	Ref.
Hf ₂ SeC	0.75	1.24	0.93	0.81	443	548	0.081	This
Hf ₂ SC	0.65	1.39	0.90	0.81	505	627	0.178	[35]
Zr ₂ SeC	0.73	1.57	1.14	0.84	383	904	0.218	[51]
Zr ₂ SC	0.73	1.34	0.98	0.85	412	955	0.113	[35]
Nb ₂ SC	0.63	1.19	0.75	0.70	530	756	0.161	[35]

In order to better comprehend the mechanical anisotropy, the directional dependent 2D projections and 3D plots of elastic properties are used to illustrate this anisotropic behavior. Fig. 3 depicts the demonstration of anisotropy in Young's and shear moduli along with linear compressibility (*K*) and Poisson's ratio (*ν*). The *Y* and *K* are isotropic in the *xy* plane while anisotropic in the *xz* and *yz* planes (Fig. 3 a and b), which are confirmed by perfectly circular (*xy* plane) and non-circular (*xz* and *yz* planes) 2D projections. In the *xy* plane, the *Y* and *K* values are

equal at the x and y axis. In the xz and yz planes, the Y_{\max} is at the 45° of horizontal and vertical axis whereas K_{\max} is at the horizontal axis (Table 4).

Table 4. Maximum and minimum values of Young's modulus, Y (GPa), linear compressibility, K (TPa^{-1}), shear modulus, G (GPa), and Poisson's ratio, ν (GPa) of M_2AC ($M = \text{Hf, Zr}$; $A = \text{Se, S}$) and Nb_2SC .

Phases	Y_{\min}	Y_{\max}	A_Y	K_{\min}	K_{\max}	A_K	G_{\min}	G_{\max}	A_G	ν_{\min}	ν_{\max}	A_ν	Ref.
Hf_2SeC	247.7	295.4	1.19	1.831	2.255	1.23	99.07	130.27	1.31	0.133	0.277	2.07	This
Hf_2SC	255.03	327.56	1.28	1.59	1.97	1.24	98.48	148.95	1.51	0.099	0.327	3.28	[35]
Zr_2SC	250.08	306.39	1.22	1.78	2.12	1.19	101.19	137.27	1.35	0.110	0.290	2.53	[35]
Zr_2SeC	208.93	277.50	1.32	1.913	2.288	1.19	81.071	127.59	1.57	0.078	0.343	4.394	[51]
Nb_2SC	217.27	297.02	1.36	1.32	1.88	1.43	88.96	128.57	1.50	0.154	0.393	2.55	[35]

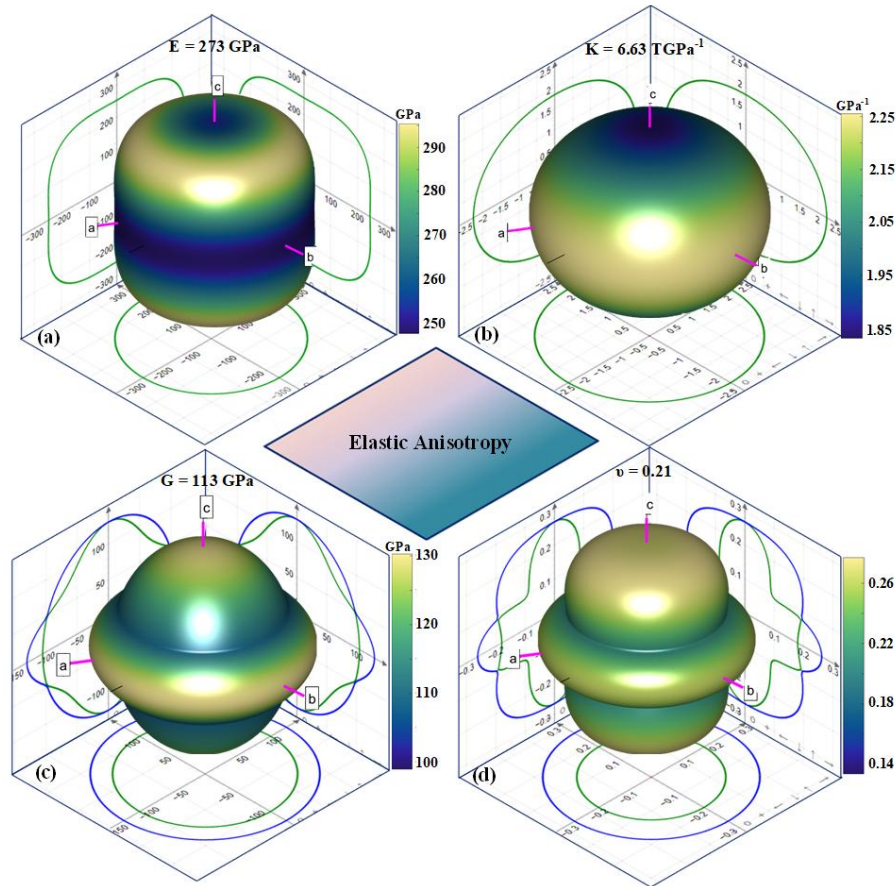


Fig. 3. The 2D projections and 3D plots of (a) Young's modulus, (b) linear compressibility, (c) shear modulus, and (d) Poisson's ratio in Hf_2SeC .

The color contrast on their 3D plots is consistent with the values in the 2D projections. The 2D projections of G and ν exhibit inner and outer surfaces (represented by green and blue lines) shown in Fig. 3 (c and d). The circular 2D projections of the inner and outer surface in xy plane reveal their isotropic nature similar to Y and K . In xz and yz planes, the outer surface of G and ν has the maximum value (G_{\max} and ν_{\max}) at the horizontal axis while the inner surface has a maximum value (G_{\max} and ν_{\max}) at the vertical axis. Due to this, the color contrast in 3D plots shows the maximum gradient at the x , y and z -axis while the minimum gradient at the 45° of the horizontal and vertical axis in the xz and yz planes. These computed values of Y , G , K , and ν are tabulated along with their anisotropic index in Table 4. This analysis shows that elastic properties are non-identical in all of the crystallographic planes and the degree of anisotropy is maximum along the z -axis. In comparison with other chalcogenide MAX phases, the level of anisotropy for Hf_2SeC is lowest [Table 4].

3.5. Thermodynamic properties

MAX phases exhibit promising high-temperature applications such as heating elements, protective coatings, electrical contacts, and have the potential for thermal barrier coatings (TBCs) [85]. It is important to disclose their thermodynamic properties for possible applications. Therefore, we used the quasi-harmonic Debye model [86,87] to compute the thermodynamic properties of Hf_2SeC in the temperature and pressure range of 0 to 1000°C and 0 to 50 GPa, respectively. The relationship of unit cell volume as a function of temperature and pressure is presented in Fig. 4. With the increase in temperature and pressure, the unit cell volume expands and contracts linearly. The expansion rate as a function of temperature is relatively less at 50 GPa as compared to at 0 GPa. Here, the calculated unit cell volume of 128.3 \AA^3 at 0 GPa and 300 K, is consistent with the equilibrium volume computed during optimization. The Grüneisen parameter (γ) for Hf_2SeC is following the same trend as unit cell volume. There is a linear increase and decrease in the Grüneisen parameter with an increase in temperature and pressure, respectively as shown in Fig. 5.

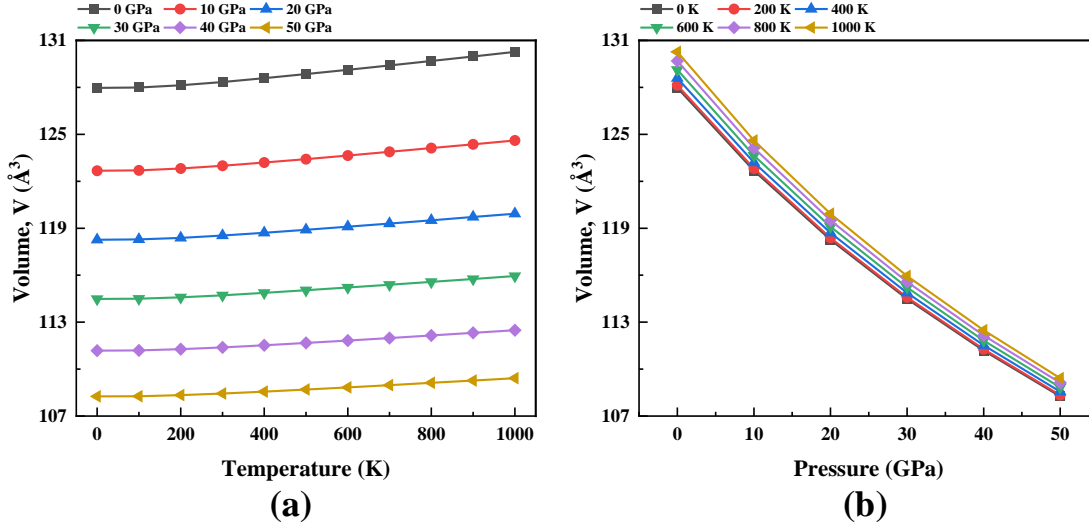


Fig. 4. Variations in unit cell volume as a function of temperature and pressure.

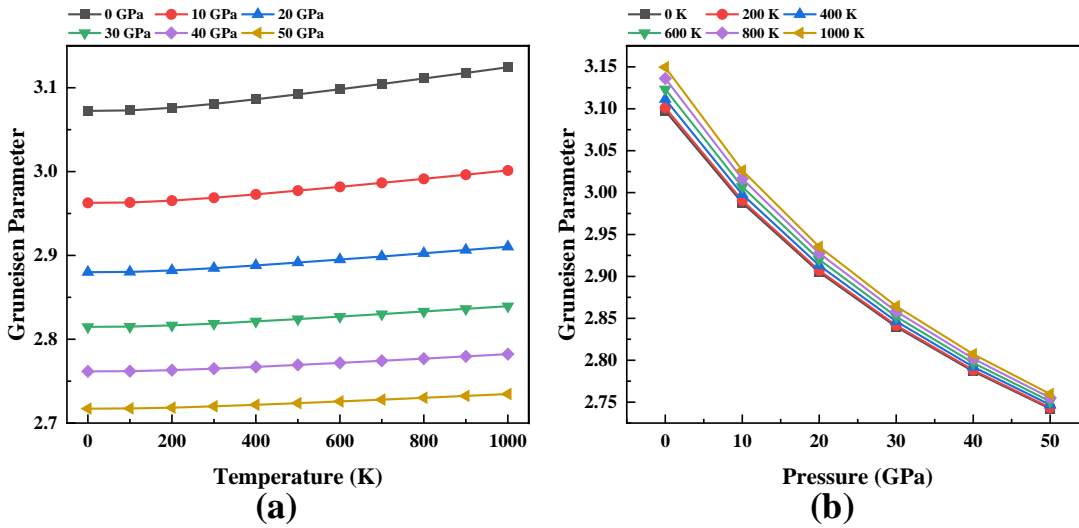


Fig. 5. Variations in Grüneisen parameter as a function of temperature and pressure.

The change in Debye temperature with the variation of temperature and pressure is illustrated in Fig. 6. It is found that the Debye temperature decreases with an increase in temperature while decreasing with an increase in pressure. At 0 GPa and 300 K, the Debye temperature of Hf_2SeC is 640 K which is comparable with its counterpart Hf_2SC (598 K)[51]. We have also computed the Debye temperature (Θ_D) using Anderson's model [88] for both Hf_2AC ($A = \text{Se}, \text{S}$). The Θ_D of Hf_2SeC (640 K, 490 K) is higher than that of Hf_2SC (598 K, 454 K), is in good agreement with the statement that higher Θ_D corresponds to the harder solids [Section 3.2, hardness of Hf_2SeC is

higher than Hf_2SeC]. Furthermore, the melting temperature of the titled phase is computed using the model [89] $T_m = 3C_{11} + 1.5C_{33} + 354$, where C_{11} and C_{33} are the elastic constants. The calculated melting point of 1674 K is comparable (slightly lower) with that of Hf_2SC (1778 K), which implies that it is also suitable for high-temperature applications. The T_m is related to Young's modulus (Y), the higher T_m is for the solids with higher Y . The obtained values also agree with the Y values (Hf_2SeC – 273 GPa and Hf_2SC – 295 GPa). Moreover, the minimum thermal conductivity is also calculated using the formula [90]: $K_{min} = k_B v_m \left(\frac{M}{n \rho N_A} \right)^{-2/3}$ where k_B , v_m , N_A , and ρ are Boltzmann constant, average phonon velocity, Avogadro's number, and density of crystal, respectively. The obtained K_{min} is 0.86 (W/mK) which is almost equal to that of Hf_2SC [0.85 (W/mK)] [35], smaller than Zr_2SeC [1.33 (W/mK)] and M_2SC ($M = \text{Zr}, \text{Nb}$) [35], also suggests for use in high temperature technology as a coating materials.

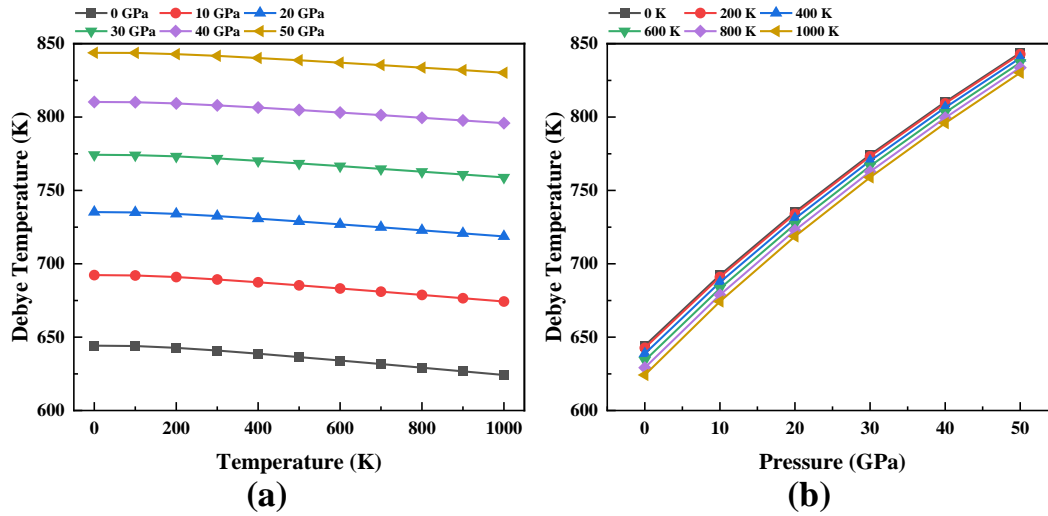


Fig. 6. Variations in Debye temperatures as a function of temperature and pressure.

In Fig. 7, the dependence of the thermal expansion coefficient (TEC) on the temperature and pressure is given. The TEC is constant at 0 K in the pressure range of 0 to 50 GPa. The TEC is increase sharply up to the temperature of 400 K, later, it increases at a gradual rate. The increase in TEC at 0 GPa is higher as compared to 50 GPa. At any constant temperature, the TEC decreases linearly with the increase in pressure. The computed TEC for Hf_2SeC is $2.66 \times 10^{-5} \text{ K}^{-1}$ is comparable with that of Zr_2SeC $3.88 \times 10^{-5} \text{ K}^{-1}$ [51]. The dependence of specific heat at constant volume (C_v) on temperature and pressure is presented in Fig. 8. The variation in C_v as a function

of temperature obeys the Debye T^3 -law and finally becomes constant to reach the classical Dulong-petit (DP) limit i.e., $C_v = 3nNk_B = 195.7 \text{ Jmol}^{-1}\text{K}^{-1}$. At 0 K, C_v remains constant while decreasing linearly at higher temperatures as a function of pressure until a temperature where C_v gets converged to reach the DP limit.

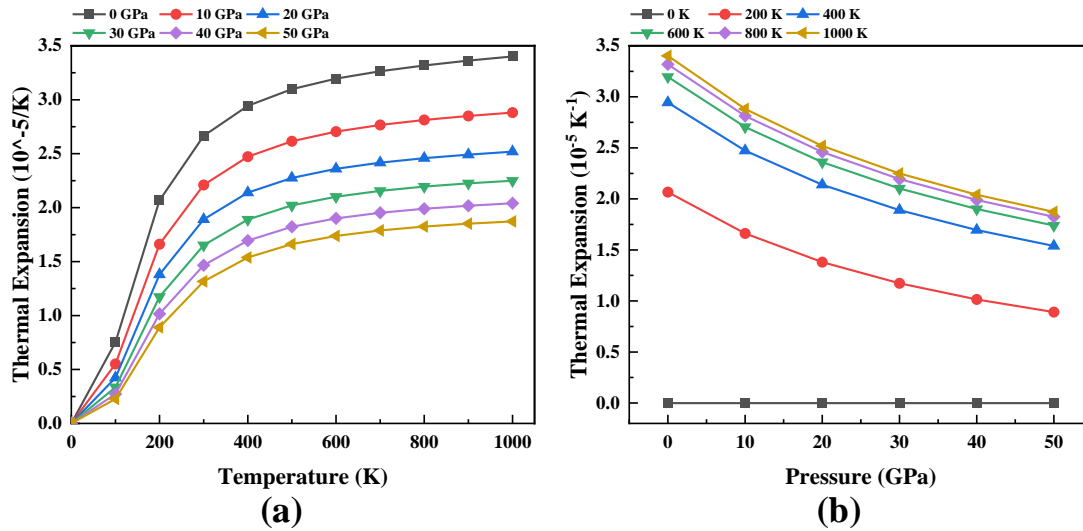


Fig. 7. Variations in thermal expansion coefficient as a function of temperature and pressure.

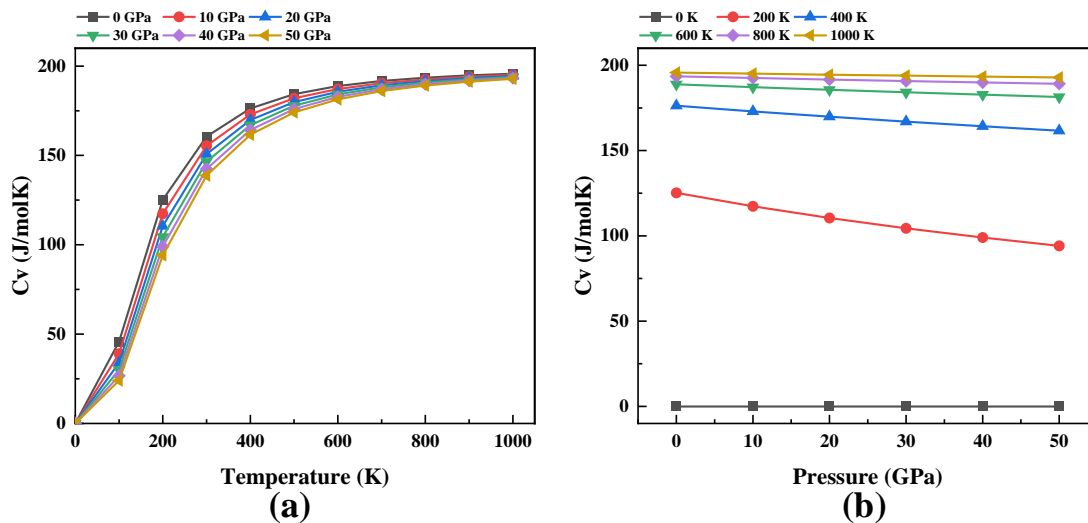


Fig. 8. Variations in specific heat at constant volume as a function of temperature and pressure.

We conclude this section as follows: a good relationship between mechanical and thermal properties is found such as higher Debye temperature for Hf_2SeC than Hf_2SC due to higher

hardness and higher melting point for Hf₂SC than Hf₂SeC due to higher Young's modulus owing to their interdependence nature. In comparison with TBC materials [91,92], the Debye temperature, melting temperature as well as minimum thermal conductivity values suggest that Hf₂SeC is like to be a possible thermal barrier coating material.

4. Conclusions

A recently synthesized chalcogenide MAX phase Hf₂SeC has been studied using the DFT-based first-principles study. The obtained lattice constants agree well with the previous results. The synthesized titled MAX phase is also mechanically stable. The unequal values of C_{11} and C_{33} imply the anisotropic nature. The obtained parameters for mechanical behavior are comparable with those of other chalcogenide MAX phases. Elastic constants and moduli of Hf₂SeC are lower than that of its precursor phase Hf₂SC while the hardness follows the reverse trend. The titled boride is like to be 2nd hardest chalcogenide MAX phase. The Hf₂SeC is brittle like other MAX phases whereas Hf₂SeC is more brittle compared to its precursor Hf₂SC. The variation of hardness among Hf₂AC (A = Se, S) is well explained in terms of DOSs. The band structure confirms the metallic nature whereas the charge density mapping discloses the mixture of covalent and ionic bonds. The electronic conductivity is anisotropic in nature. Different anisotropic indices, and 2D and 3D plots of Y , B , G , and ν also revealed the anisotropic behavior of the mechanical properties. The variation of the thermal properties with temperature and pressure follows the usual trend. The estimated Debye temperature, melting point, and minimum thermal conductivity reveal the possibility of Hf₂SeC to be used in high-temperature technology as a TBC material. It is expected that the present study will stimulate the scientific community to discover more Se-based MAX phases in the future.

Conflicts of interest

The authors declare no conflicts of interest.

Funding: This research did not receive any specific grant from funding agencies in the public, commercial, or not-for-profit sectors.

References

- [1] K. Chen, X. Bai, X. Mu, P. Yan, N. Qiu, Y. Li, J. Zhou, Y. Song, Y. Zhang, S. Du, Z. Chai, Q. Huang, MAX phase Zr₂SeC and its thermal conduction behavior, *J. Eur. Ceram. Soc.* 41 (2021) 4447–4451. <https://doi.org/10.1016/j.jeurceramsoc.2021.03.013>.

- [2] X. Wang, K. Chen, E. Wu, Y. Zhang, H. Ding, N. Qiu, Y. Song, S. Du, Z. Chai, Q. Huang, Synthesis and thermal expansion of chalcogenide MAX phase Hf₂SeC, *J. Eur. Ceram. Soc.* 42 (2022) 2084–2088. <https://doi.org/10.1016/j.jeurceramsoc.2021.12.062>.
- [3] M. Sokol, V. Natu, S. Kota, M.W. Barsoum, On the Chemical Diversity of the MAX Phases, *Trends Chem.* 1 (2019) 210–223. <https://doi.org/10.1016/j.trechm.2019.02.016>.
- [4] S. Kuchida, T. Muranaka, K. Kawashima, K. Inoue, M. Yoshikawa, J. Akimitsu, Superconductivity in Lu₂SnC, *Phys. C Supercond.* 494 (2013) 77–79. <https://doi.org/10.1016/j.physc.2013.04.050>.
- [5] T. Rackl, D. Johrendt, The MAX phase borides Zr₂SB and Hf₂SB, *Solid State Sci.* 106 (2020) 106316. <https://doi.org/10.1016/j.solidstatesciences.2020.106316>.
- [6] T. Rackl, L. Eisenburger, R. Niklaus, D. Johrendt, Syntheses and physical properties of the MAX phase boride Nb₂SB and the solid solutions Nb₂S_xC_{1-x} (x=0–1), *Phys. Rev. Mater.* 3 (2019) 054001. <https://doi.org/10.1103/PhysRevMaterials.3.054001>.
- [7] H. Ding, Y. Li, J. Lu, K. Luo, K. Chen, M. Li, P.O.Å. Persson, L. Hultman, P. Eklund, S. Du, Z. Huang, Z. Chai, H. Wang, P. Huang, Q. Huang, Synthesis of MAX phases Nb₂CuC and Ti₂(Al_{0.1}Cu_{0.9})N by A-site replacement reaction in molten salts, *Mater. Res. Lett.* 7 (2019) 510–516. <https://doi.org/10.1080/21663831.2019.1672822>.
- [8] L. Mian, L. You-Bing, L. Kan, L. Jun, E. Per, P. Per, R. Johanna, H. Lars, D. Shi-Yu, H. Zheng-Ren, H. Qing, Synthesis of Novel MAX Phase Ti₃ZnC₂ via A-site-element-substitution Approach, *J. Inorg. Mater.* 34 (2019) 60. <https://doi.org/10.15541/jim20180377>.
- [9] M. Li, J. Lu, K. Luo, Y. Li, K. Chang, K. Chen, J. Zhou, J. Rosen, L. Hultman, P. Eklund, P.O.Å. Persson, S. Du, Z. Chai, Z. Huang, Q. Huang, Element Replacement Approach by Reaction with Lewis Acidic Molten Salts to Synthesize Nanolaminated MAX Phases and MXenes, *J. Am. Chem. Soc.* 141 (2019) 4730–4737. <https://doi.org/10.1021/jacs.9b00574>.
- [10] H. Fashandi, M. Dahlqvist, J. Lu, J. Palisaitis, S.I. Simak, I.A. Abrikosov, J. Rosen, L. Hultman, M. Andersson, A. Lloyd Spetz, P. Eklund, Synthesis of Ti₃AuC₂, Ti₃Au₂C₂ and Ti₃IrC₂ by noble metal substitution reaction in Ti₃SiC₂ for high-temperature-stable Ohmic contacts to SiC, *Nat. Mater.* 16 (2017) 814–818. <https://doi.org/10.1038/nmat4896>.
- [11] Y. Li, Y. Qin, K. Chen, L. Chen, X. Zhang, H. Ding, M. Li, Y. Zhang, S. Du, Z. Chai, Q. Huang, Molten Salt Synthesis of Nanolaminated Sc₂SnC MAX Phase, *Wuji Cailiao Xuebao/Journal Inorg. Mater.* 36 (2021) 773–778. <https://doi.org/10.15541/jim20200529>.
- [12] B. Tunca, T. Lapauw, O.M. Karakulina, M. Batuk, T. Cabioc'h, J. Hadermann, R. Delville, K. Lambrinou, J. Vleugels, Synthesis of MAX Phases in the Zr-Ti-Al-C System, *Inorg. Chem.* 56 (2017) 3489–3498. <https://doi.org/10.1021/acs.inorgchem.6b03057>.
- [13] T. Lapauw, B. Tunca, D. Potashnikov, A. Pesach, O. Ozeri, J. Vleugels, K. Lambrinou, The double solid solution (Zr, Nb)₂(Al, Sn)C MAX phase: a steric stability approach, *Sci. Rep.* 8 (2018) 12801. <https://doi.org/10.1038/s41598-018-31271-2>.

- [14] B. Tunca, T. Lapauw, R. Delville, D.R. Neuville, L. Hennet, D. Thiaudière, T. Ouisse, J. Hadermann, J. Vleugels, K. Lambrinou, Synthesis and Characterization of Double Solid Solution (Zr,Ti)₂(Al,Sn)C MAX Phase Ceramics, *Inorg. Chem.* 58 (2019) 6669–6683. <https://doi.org/10.1021/acs.inorgchem.9b00065>.
- [15] M. Griseri, B. Tunca, S. Huang, M. Dahlqvist, J. Rosén, J. Lu, P.O.Å. Persson, L. Popescu, J. Vleugels, K. Lambrinou, Ta-based 413 and 211 MAX phase solid solutions with Hf and Nb, *J. Eur. Ceram. Soc.* 40 (2020) 1829–1838. <https://doi.org/10.1016/j.jeurceramsoc.2019.12.052>.
- [16] E.Z.S.G. Christopoulos, N. Ni, D.C. Par, D. Horlait, M.E. Fitzpatrick, A. Chroneos, W.E. Lee, Experimental synthesis and density functional theory investigation of radiation tolerance of Zr₃(Al_{1-x}Si_x)C₂ MAX phases, (2017) 1–11. <https://doi.org/10.1111/jace.14742>.
- [17] R. Pan, J. Zhu, Y. Liu, Synthesis, microstructure and properties of (Ti_{1-x}, Mo_x)₂AlC phases, *Mater. Sci. Technol.* 34 (2018) 1064–1069. <https://doi.org/10.1080/02670836.2017.1419614>.
- [18] C. Zuo, C. Zhong, Screen the elastic and thermodynamic properties of MAX solid solution using DFT procedure: Case study on (Ti_{1-x}V_x)₂AlC, *Mater. Chem. Phys.* (2020) 123059. <https://doi.org/10.1016/j.matchemphys.2020.123059>.
- [19] M.A. Ali, S.H. Naqib, Recently synthesized (Ti_{1-x}Mo_x)₂AlC (0 ≤ x ≤ 0.20) solid solutions: deciphering the structural, electronic, mechanical and thermodynamic properties via ab initio simulations, *RSC Adv.* 10 (2020) 31535–31546. <https://doi.org/10.1039/D0RA06435A>.
- [20] C.M. Hamm, J.D. Bocarsly, G. Seward, U.I. Kramm, C.S. Birkel, Non-conventional synthesis and magnetic properties of MAX phases (Cr/Mn)₂AlC and (Cr/Fe)₂AlC, *J. Mater. Chem. C.* 5 (2017). <https://doi.org/10.1039/c7tc00112f>.
- [21] M.A. Ali, Newly Synthesized Ta- Based MAX Phase (Ta_{1-x}Hf_x)₄AlC₃ and (Ta_{1-x}Hf_x)₄Al_{0.5}Sn_{0.5}C₃ (0 ≤ x ≤ 0.25) Solid Solutions: Unravelling the Mechanical, Electronic, and Thermodynamic Properties, *Phys. Status Solidi.* 258 (2021) 2000307. <https://doi.org/10.1002/pssb.202000307>.
- [22] M.A. Ali, M.R. Khatun, N. Jahan, M.M. Hossain, Comparative study of Mo₂Ga₂C with superconducting MAX phase Mo₂GaC: First-principles calculations, *Chinese Phys. B.* 26 (2017) 033102. <https://doi.org/10.1088/1674-1056/26/3/033102>.
- [23] C. Hu, C.-C. Lai, Q. Tao, J. Lu, J. Halim, L. Sun, J. Zhang, J. Yang, B. Anasori, J. Wang, Y. Sakka, L. Hultman, P. Eklund, J. Rosen, M.W. Barsoum, Mo₂Ga₂C: a new ternary nanolaminated carbide, *Chem. Commun.* 51 (2015) 6560–6563. <https://doi.org/10.1039/C5CC00980D>.
- [24] H. He, S. Jin, G. Fan, L. Wang, Q. Hu, A. Zhou, Synthesis mechanisms and thermal stability of ternary carbide Mo₂Ga₂C, *Ceram. Int.* 44 (2018) 22289–22296. <https://doi.org/10.1016/j.ceramint.2018.08.353>.

- [25] H. Chen, D. Yang, Q. Zhang, S. Jin, L. Guo, J. Deng, X. Li, X. Chen, A Series of MAX Phases with MA-Triangular-Prism Bilayers and Elastic Properties, *Angew. Chemie - Int. Ed.* 58 (2019) 4576–4580. <https://doi.org/10.1002/anie.201814128>.
- [26] Q. Tao, J. Lu, M. Dahlqvist, A. Mockute, S. Calder, A. Petruhins, R. Meshkian, O. Rivin, D. Potashnikov, E.N. Caspi, H. Shaked, A. Hoser, C. Opagiste, R.-M. Galera, R. Salikhov, U. Wiedwald, C. Ritter, A.R. Wildes, B. Johansson, L. Hultman, M. Farle, M.W. Barsoum, J. Rosen, Atomically Layered and Ordered Rare-Earth i -MAX Phases: A New Class of Magnetic Quaternary Compounds, *Chem. Mater.* 31 (2019) 2476–2485. <https://doi.org/10.1021/acs.chemmater.8b05298>.
- [27] L. Chen, M. Dahlqvist, T. Lapauw, B. Tunca, F. Wang, J. Lu, R. Meshkian, K. Lambrinou, B. Blanpain, J. Vleugels, J. Rosen, Theoretical Prediction and Synthesis of $(\text{Cr}_{2/3}\text{Zr}_{1/3})_2\text{AlC}$ i -MAX Phase, *Inorg. Chem.* 57 (2018) 6237–6244. <https://doi.org/10.1021/acs.inorgchem.8b00021>.
- [28] N. Miao, J. Wang, Y. Gong, J. Wu, H. Niu, S. Wang, K. Li, A.R. Oganov, T. Tada, H. Hosono, Computational Prediction of Boron-Based MAX Phases and MXene Derivatives, *Chem. Mater.* 32 (2020) 6947–6957. <https://doi.org/10.1021/acs.chemmater.0c02139>.
- [29] J. Wang, T.N. Ye, Y. Gong, J. Wu, N. Miao, T. Tada, H. Hosono, Discovery of hexagonal ternary phase Ti_2InB_2 and its evolution to layered boride TiB , *Nat. Commun.* 10 (2019) 1–8. <https://doi.org/10.1038/s41467-019-10297-8>.
- [30] M.A. Ali, M.M. Hossain, M.M. Uddin, A.K.M.A. Islam, D. Jana, S.H. Naqib, DFT insights into new B-containing 212 MAX phases: Hf_2AB_2 ($A = \text{In}, \text{Sn}$), *J. Alloys Compd.* 860 (2021) 158408. <https://doi.org/10.1016/j.jallcom.2020.158408>.
- [31] M.A. Ali, M.M. Hossain, M.M. Uddin, A.K.M.A. Islam, S.H. Naqib, Understanding the improvement of thermo-mechanical and optical properties of 212 MAX phase borides Zr_2AB_2 ($A = \text{In}, \text{Tl}$), *J. Mater. Res. Technol.* 15 (2021) 2227–2241. <https://doi.org/10.1016/j.jmrt.2021.09.042>.
- [32] M.A. Ali, M.M. Hossain, A.K.M.A. Islam, S.H. Naqib, Ternary boride Hf_3PB_4 : Insights into the physical properties of the hardest possible boride MAX phase, *J. Alloys Compd.* 857 (2021) 158264. <https://doi.org/10.1016/j.jallcom.2020.158264>.
- [33] M.W. Qureshi, M.A. Ali, X. Ma, Screen the thermomechanical and optical properties of the new ductile 314 MAX phase boride Zr_3CdB_4 : A DFT insight, *J. Alloys Compd.* 877 (2021) 160248. <https://doi.org/10.1016/j.jallcom.2021.160248>.
- [34] P. Chakraborty, A. Chakrabarty, A. Dutta, T. Saha-Dasgupta, Soft MAX phases with boron substitution: A computational prediction, *Phys. Rev. Mater.* 2 (2018) 103605. <https://doi.org/10.1103/PhysRevMaterials.2.103605>.
- [35] M.A. Ali, M.M. Hossain, M.M. Uddin, M.A. Hossain, A.K.M.A. Islam, S.H. Naqib, Physical properties of new MAX phase borides $M_2\text{SB}$ ($M = \text{Zr}, \text{Hf}$ and Nb) in comparison with conventional MAX phase carbides $M_2\text{SC}$ ($M = \text{Zr}, \text{Hf}$ and Nb): Comprehensive insights, *J. Mater. Res. Technol.* 11 (2021) 1000–1018.

<https://doi.org/10.1016/j.jmrt.2021.01.068>.

- [36] M. Khazaei, M. Arai, T. Sasaki, M. Estili, Y. Sakka, Trends in electronic structures and structural properties of MAX phases: a first-principles study on M_2AlC ($M = Sc, Ti, Cr, Zr, Nb, Mo, Hf, \text{ or } Ta$), M_2AlN , and hypothetical M_2AlB phases, *J. Phys. Condens. Matter.* 26 (2014) 505503. <https://doi.org/10.1088/0953-8984/26/50/505503>.
- [37] G. Surucu, B. Yildiz, A. Erkisi, X. Wang, O. Surucu, The investigation of electronic, anisotropic elastic and lattice dynamical properties of MAB phase nanolaminated ternary borides: M_2AlB_2 ($M=Mn, Fe \text{ and } Co$) under spin effects, *J. Alloys Compd.* 838 (2020). <https://doi.org/10.1016/j.jallcom.2020.155436>.
- [38] A. Gencer, G. Surucu, Electronic and lattice dynamical properties of Ti_2SiB MAX phase, *Mater. Res. Express.* 5 (2018) 076303. <https://doi.org/10.1088/2053-1591/aace7f>.
- [39] G. Surucu, Investigation of structural, electronic, anisotropic elastic, and lattice dynamical properties of MAX phases borides: An Ab-initio study on hypothetical M_2AB ($M = Ti, Zr, Hf; A = Al, Ga, In$) compounds, *Mater. Chem. Phys.* 203 (2018) 106–117. <https://doi.org/10.1016/j.matchemphys.2017.09.050>.
- [40] M. Barsoum, T. El-Raghy, The MAX Phases: Unique New Carbide and Nitride Materials, *Am. Sci.* 89 (2001) 334. <https://doi.org/10.1511/2001.4.334>.
- [41] G. Qing-He, X. Zhi-Jun, T. Ling, Z. Xianjun, J. Guozhu, D. An, L. Rong-Feng, G. Yun-Dong, Y. Ze-Jin, Evidence of the stability of Mo_2TiAlC_2 from first principles calculations and its thermodynamical and optical properties, *Comput. Mater. Sci.* 118 (2016) 77–86. <https://doi.org/10.1016/J.COMMATSCI.2016.03.010>.
- [42] M.W. Barsoum, MAX phases: Properties of machinable ternary carbides and nitrides, Wiley-VCH Verlag GmbH & Co. KGaA, Weinheim, Germany, 2013. <https://doi.org/10.1002/9783527654581>.
- [43] M.R. Khatun, M.A. Ali, F. Parvin, A.K.M.A. Islam, Elastic, thermodynamic and optical behavior of V_2AC ($A = Al, Ga$) MAX phases, *Results Phys.* 7 (2017) 3634–3639. <https://doi.org/10.1016/j.rinp.2017.09.043>.
- [44] A.S. Ingason, M. Dahlqvist, J. Rosen, Magnetic MAX phases from theory and experiments; A review, *J. Phys. Condens. Matter.* (2016). <https://doi.org/10.1088/0953-8984/28/43/433003>.
- [45] A. Bouhemadou, R. Khenata, Structural, electronic and elastic properties of M_2SC ($M=Ti, Zr, Hf$) compounds, *Phys. Lett. A.* 372 (2008) 6448–6452. <https://doi.org/10.1016/j.physleta.2008.08.066>.
- [46] I.R. Shein, A.L. Ivanovskii, Elastic properties of superconducting MAX phases from first-principles calculations, *Phys. Status Solidi.* 248 (2011) 228–232. <https://doi.org/10.1002/pssb.201046163>.
- [47] E. Karaca, P. Byrne, P. Hasnip, H.M. Tutuncu, M. Probert, Electron-Phonon Interaction and Superconductivity in Hexagonal Ternary Carbides Nb_2AC ($A: Al, S, Ge, As \text{ and } Sn$),

- Electron. Struct. (2021). <https://doi.org/10.1088/2516-1075/ac2c94>.
- [48] M.T. Nasir, M.A. Hadi, S.H. Naqib, F. Parvin, A.K.M.A. Islam, M. Roknuzzaman, M.S. Ali, Zirconium metal-based MAX phases Zr_2AC ($A = Al, Si, P$ and S): A first-principles study, 28 (2014) 1–16. <https://doi.org/10.1142/S0217979215500228>.
- [49] M.T. Nasir, A.K.M.A. Islam, MAX phases Nb_2AC ($A = S, Sn$): An ab initio study, Comput. Mater. Sci. 65 (2012) 365–371. <https://doi.org/10.1016/J.COMMATSCI.2012.08.003>.
- [50] M.F. Cover, O. Warschkow, M.M.M. Bilek, D.R. McKenzie, A comprehensive survey of M_2AX phase elastic properties, J. Phys. Condens. Matter. 21 (2009) 305403. <https://doi.org/10.1088/0953-8984/21/30/305403>.
- [51] M.A. Ali, M.W. Qureshi, Newly synthesized MAX phase Zr_2SeC : DFT insights into physical properties towards possible applications, RSC Adv. 11 (2021) 16892–16905. <https://doi.org/10.1039/d1ra02345d>.
- [52] W.-K. Pang, I.M. Low, Understanding and improving the thermal stability of layered ternary carbides and nitrides, in: Adv. Ceram. Matrix Compos., Elsevier, 2018: pp. 429–460. <https://doi.org/10.1016/B978-0-08-102166-8.00018-9>.
- [53] Y. Fu, B. Wang, Y. Teng, X. Zhu, X. Feng, M. Yan, P. Korzhavyi, W. Sun, The role of group III, IV elements in Nb_4AC_3 MAX phases ($A = Al, Si, Ga, Ge$) and the unusual anisotropic behavior of the electronic and optical properties, Phys. Chem. Chem. Phys. 19 (2017) 15471–15483. <https://doi.org/10.1039/C7CP01375B>.
- [54] M.M. Ali, M.A. Hadi, I. Ahmed, A.F.M.Y. Haider, A.K.M.A. Islam, Physical properties of a novel boron-based ternary compound Ti_2InB_2 , Mater. Today Commun. 25 (2020) 101600. <https://doi.org/10.1016/j.mtcomm.2020.101600>.
- [55] M.A. Hadi, M. Dahlqvist, S.-R.G. Christopoulos, S.H. Naqib, A. Chroneos, A.K.M.A. Islam, Chemically stable new MAX phase V_2SnC : a damage and radiation tolerant TBC material, RSC Adv. 10 (2020) 43783–43798. <https://doi.org/10.1039/D0RA07730E>.
- [56] M.D. Segall, P.J.D. Lindan, M.J. Probert, C.J. Pickard, P.J. Hasnip, S.J. Clark, M.C. Payne, First-principles simulation: ideas, illustrations and the CASTEP code, J. Phys. Condens. Matter. 14 (2002) 2717–2744. <https://doi.org/10.1088/0953-8984/14/11/301>.
- [57] S.J. Clark, M.D. Segall, C.J. Pickard, P.J. Hasnip, M.I.J. Probert, K. Refson, M.C. Payne, First principles methods using CASTEP, Zeitschrift Für Krist. - Cryst. Mater. 220 (2005). <https://doi.org/10.1524/zkri.220.5.567.65075>.
- [58] J.P. Perdew, K. Burke, M. Ernzerhof, Generalized Gradient Approximation Made Simple, Phys. Rev. Lett. 77 (1996) 3865–3868. <https://doi.org/10.1103/PhysRevLett.77.3865>.
- [59] H.J. Monkhorst, J.D. Pack, Special points for Brillouin-zone integrations, Phys. Rev. B. 13 (1976) 5188–5192. <https://doi.org/10.1103/PhysRevB.13.5188>.
- [60] M.W. Barsoum, The $MN_{n+1}AX_n$ phases: A new class of solids, Prog. Solid State Chem.

- 28 (2000) 201–281. [https://doi.org/10.1016/S0079-6786\(00\)00006-6](https://doi.org/10.1016/S0079-6786(00)00006-6).
- [61] Y.X. Wang, Z.X. Yan, W. Liu, G.L. Zhou, Structure stability, mechanical properties and thermal conductivity of the new hexagonal ternary phase Ti_2InB_2 under pressure, *Philos. Mag.* 100 (2020) 2054–2067. <https://doi.org/10.1080/14786435.2020.1754485>.
- [62] Y. Medkour, A. Bouhemadou, A. Roumili, Structural and electronic properties of M_2InC ($\text{M} = \text{Ti}, \text{Zr}, \text{and Hf}$), *Solid State Commun.* 148 (2008) 459–463. <https://doi.org/10.1016/j.ssc.2008.09.006>.
- [63] M.W. Qureshi, X. Ma, G. Tang, R. Paudel, Ab initio predictions of structure and physical properties of the Zr_2GaC and Hf_2GaC MAX- phases under pressure, *Sci. Reports* |. 11 (2021) 1–23. <https://doi.org/10.1038/s41598-021-82402-1>.
- [64] M. Born, On the stability of crystal lattices. I, *Math. Proc. Cambridge Philos. Soc.* 36 (1940) 160–172. <https://doi.org/10.1017/S0305004100017138>.
- [65] F. Mouhat, F.-X. Coudert, Necessary and sufficient elastic stability conditions in various crystal systems, *Phys. Rev. B.* 90 (2014) 224104. <https://doi.org/10.1103/PhysRevB.90.224104>.
- [66] R. Hill, The Elastic Behaviour of a Crystalline Aggregate, *Proc. Phys. Soc. Sect. A.* 65 (1952) 349–354. <https://doi.org/10.1088/0370-1298/65/5/307>.
- [67] W. Voigt, *Lehrbuch der Kristallphysik*, Vieweg+Teubner Verlag, Wiesbaden, 1966. <https://doi.org/10.1007/978-3-663-15884-4>.
- [68] A. Reuss, Berechnung der Fließgrenze von Mischkristallen auf Grund der Plastizitätsbedingung für Einkristalle., *ZAMM - J. Appl. Math. Mech. / Zeitschrift Für Angew. Math. Und Mech.* 9 (1929) 49–58. <https://doi.org/10.1002/zamm.19290090104>.
- [69] X.-Q. Chen, H. Niu, D. Li, Y. Li, Modeling hardness of polycrystalline materials and bulk metallic glasses, *Intermetallics.* 19 (2011) 1275–1281. <https://doi.org/10.1016/j.intermet.2011.03.026>.
- [70] N. Miao, B. Sa, J. Zhou, Z. Sun, Theoretical investigation on the transition-metal borides with Ta_3B_4 -type structure: A class of hard and refractory materials, *Comput. Mater. Sci.* 50 (2011) 1559–1566. <https://doi.org/10.1016/J.COMMATSCI.2010.12.015>.
- [71] Y. Pan, X. Wang, S. Li, Y. Li, M. Wen, DFT prediction of a novel molybdenum tetraboride superhard material, *RSC Adv.* 8 (2018) 18008–18015. <https://doi.org/10.1039/c8ra02324g>.
- [72] S.F. Pugh, XCII. Relations between the elastic moduli and the plastic properties of polycrystalline pure metals, London, Edinburgh, Dublin *Philos. Mag. J. Sci.* 45 (1954) 823–843. <https://doi.org/10.1080/14786440808520496>.
- [73] M. Roknuzzaman, M.A. Hadi, M.A. Ali, M.M. Hossain, N. Jahan, M.M. Uddin, J.A. Alarco, K. Ostrikov, First hafnium-based MAX phase in the 312 family, Hf_3AlC_2 : A first-principles study, *J. Alloys Compd.* 727 (2017) 616–626.

<https://doi.org/10.1016/j.jallcom.2017.08.151>.

- [74] D.G. Pettifor, Theoretical predictions of structure and related properties of intermetallics, *Mater. Sci. Technol.* 8 (1992) 345–349. <https://doi.org/10.1179/026708392790170801>.
- [75] M.A. Ali, M.M. Hossain, M.A. Hossain, M.T. Nasir, M.M. Uddin, M.Z. Hasan, A.K.M.A. Islam, S.H. Naqib, Recently synthesized $(\text{Zr}_{1-x}\text{Ti}_x)_2\text{AlC}$ ($0 \leq x \leq 1$) solid solutions: Theoretical study of the effects of M mixing on physical properties, *J. Alloys Compd.* 743 (2018) 146–154. <https://doi.org/10.1016/j.jallcom.2018.01.396>.
- [76] Y. Zhou, Z. Sun, Electronic structure and bonding properties of layered machinable and ceramics, *Phys. Rev. B - Condens. Matter Mater. Phys.* 61 (2000) 12570–12573. <https://doi.org/10.1103/PhysRevB.61.12570>.
- [77] J. Wang, Y. Zhou, Dependence of elastic stiffness on electronic band structure of nanolaminate M_2AlC ($\text{M} = \text{Ti}, \text{V}, \text{Nb}, \text{and Cr}$) ceramics, 214111 (2004) 1–9. <https://doi.org/10.1103/PhysRevB.69.214111>.
- [78] Y.Y. Liu, Y.X. Wang, Z.X. Yan, W. Liu, G.L. Zhou, K.Z. Xiong, J.B. Gu, Pressure effects on structure, mechanical properties and thermal conductivity of V_2SnC : a first-principles study, *Philos. Mag.* 0 (2021) 1–16. <https://doi.org/10.1080/14786435.2021.1988747>.
- [79] M.W. Qureshi, X. Ma, G. Tang, R. Paudel, Ab initio predictions of structure and physical properties Hf_2GaC MAX of the - Zr_2GaC and - phases under pressure, (2021) 1–24. <https://doi.org/10.1038/s41598-021-82402-1>.
- [80] W. Sailuam, I. Fongkaew, S. Limpijumnong, K. Phacheerak, A first principles investigation on the structural, elastic, and mechanical properties of MAX phase M_3AlC_2 ($\text{M} = \text{Ta}, \text{Ti}, \text{V}$) as a function of pressure, *Comput. Condens. Matter.* 30 (2022) e00638. <https://doi.org/10.1016/j.cocom.2021.e00638>.
- [81] H.M. Ledbetter, Elastic properties of zinc: A compilation and a review, *J. Phys. Chem. Ref. Data.* 6 (1977) 1181–1203. <https://doi.org/10.1063/1.555564>.
- [82] A.K.M.A. Islam, A.S. Sikder, F.N. Islam, NbB_2 : a density functional study, *Phys. Lett. A.* 350 (2006) 288–292. <https://doi.org/10.1016/j.physleta.2005.09.085>.
- [83] J. Wang, Y. Zhou, T. Liao, Z. Lin, First-principles prediction of low shear-strain resistance of Al_3BC_3 : A metal borocarbide containing short linear BC_2 units, *Appl. Phys. Lett.* 89 (2006) 021917. <https://doi.org/10.1063/1.2220549>.
- [84] S.I. Ranganathan, M. Ostoja-Starzewski, Universal Elastic Anisotropy Index, *Phys. Rev. Lett.* 101 (2008) 055504. <https://doi.org/10.1103/PhysRevLett.101.055504>.
- [85] J. Gonzalez-Julian, Processing of MAX phases: From synthesis to applications, *J. Am. Ceram. Soc.* 104 (2021) 659–690. <https://doi.org/10.1111/jace.17544>.
- [86] A. Otero-De-La-Roza, D. Abbasi-Pérez, V. Luaña, Gibbs2: A new version of the quasiharmonic model code. II. Models for solid-state thermodynamics, features and

- implementation, *Comput. Phys. Commun.* 182 (2011) 2232–2248.
<https://doi.org/10.1016/j.cpc.2011.05.009>.
- [87] M.A. Blanco, E. Francisco, V. Luaña, GIBBS: Isothermal-isobaric thermodynamics of solids from energy curves using a quasi-harmonic Debye model, *Comput. Phys. Commun.* 158 (2004) 57–72. <https://doi.org/10.1016/j.comphy.2003.12.001>.
- [88] O.L. Anderson, A simplified method for calculating the debye temperature from elastic constants, *J. Phys. Chem. Solids.* 24 (1963) 909–917. [https://doi.org/10.1016/0022-3697\(63\)90067-2](https://doi.org/10.1016/0022-3697(63)90067-2).
- [89] M.E. Fine, L.D. Brown, H.L. Marcus, Elastic constants versus melting temperature in metals, *Scr. Metall.* 18 (1984) 951–956. [https://doi.org/10.1016/0036-9748\(84\)90267-9](https://doi.org/10.1016/0036-9748(84)90267-9).
- [90] G.A. Slack, The Thermal Conductivity of Nonmetallic Crystals, *Solid State Phys. - Adv. Res. Appl.* 34 (1979) 1–71. [https://doi.org/10.1016/S0081-1947\(08\)60359-8](https://doi.org/10.1016/S0081-1947(08)60359-8).
- [91] Y. Zhou, X. Lu, H. Xiang, Z. Feng, Preparation, mechanical, and thermal properties of a promising thermal barrier material: Y4Al2O9, *J. Adv. Ceram.* 4 (2015) 94–102. <https://doi.org/10.1007/s40145-015-0141-5>.
- [92] Y. Zhou, H. Xiang, X. Lu, Z. Feng, Z. Li, Theoretical prediction on mechanical and thermal properties of a promising thermal barrier material: Y4Al2O9, *J. Adv. Ceram.* 4 (2015) 83–93. <https://doi.org/10.1007/s40145-015-0140-6>.